A late Middle Pleistocene Denisovan mandible from the Tibetan Plateau

Fahu Chen[1,2]§*, Frido Welker[3,4]§, Chuan-Chou Shen[5,6]§, Shara E. Bailey[3,7], Inga Bergmann[3], Simon Davis[8], Huan Xia[2], Hui Wang[9], Roman Fischer[8], Sarah Freidline[3], Tsai-Luen Yu[5,6], Matthew M. Skinner[3,10], Stefanie Stelzer[3,11], Guangrong Dong[2], Qiaomei Fu[12], Guanghui Dong[2], Jian Wang[2], Dongju Zhang[2]* & Jean-Jacques Hublin[3,13]*

1 Key Laboratory of Alpine Ecology (LAE), CAS Center for Excellence in Tibetan Plateau Earth System Sciences, Institute of Tibetan Plateau Research, Chinese Academy of Sciences, Beijing 100101, CHINA.

2 Key Laboratory of Western China's Environmental Systems (Ministry of Education), Center for Pan Third Pole Environment (Pan-TPE), Lanzhou University, Lanzhou 730000, CHINA.

3 Department of Human Evolution, Max Planck Institute for Evolutionary Anthropology, Deutscher Platz 6, Leipzig 04103, GERMANY.

4 Natural History Museum of Denmark, University of Copenhagen, Øster Voldgade 5-7, 1350, Copenhagen, DENMARK.

5 High-Precision Mass Spectrometry and Environment Change Laboratory (HISPEC), Department of Geosciences, National Taiwan University, Taipei 10617, Taiwan, CHINA.

6 Research Center for Future Earth, National Taiwan University, Taipei 10617, Taiwan, CHINA.

7 Department of Anthropology, Center for the Study of Human Origins, New York University, New York, NY 10003, USA.

8 Target Discovery Institute, University of Oxford, Oxford, OX3 7BN, UNITED KINGDOM.

9 Gansu Provincial Institute of Cultural Relics and Archaeological Research, Lanzhou 730000, CHINA.

10 School of Anthropology and Conservation, University of Kent, Canterbury CT2 7NR, UNITED KINGDOM.

11 Department of Anatomy and Biomechanics, Karl Landsteiner University of Health Sciences, 3500 Krems an der Donau, AUSTRIA.

12 Key Laboratory of Vertebrate Evolution and Human Origins, Institute of Vertebrate Paleontology and Paleoanthropology, Chinese Academy of Sciences, Beijing 100044, CHINA.

13 Chaire Internationale de Paléoanthropologie, Collège de France, 75005 Paris, FRANCE

§These authors contribute equally.

*Correspondence to: fhchen@itpcas.ac.cn; djzhang@lzu.edu.cn; hublin@eva.mpg.de

Denisovans are members of a hominin group only known from fragmentary fossils genomically studied from a single site, Denisova Cave[1–3] in Siberia, and from their genetic legacy through gene flow into several low-altitude East Asian populations[4,5] and high-altitude modern Tibetans[6]. The lack of morphologically informative Denisovan fossils impedes our ability to connect geographically and temporally dispersed Asian fossil hominins and understand their relation to these recent populations in a coherent manner, including the Denisovan-inherited human adaptation to the high-altitude Tibetan Plateau[7,8]. Here we report a Denisovan mandible, identified by ancient protein analysis[9,10], found in Baishiya Karst Cave, Xiahe County, Gansu Province (China), on the Tibetan Plateau. We determine the mandible to be at least 160 thousand years old through U-series dating of an adhering carbonate matrix. It is the first direct evidence of this hominin group outside the Altai Mountains, and provides unique insights into Denisovan mandibular and dental morphology. Our results indicate that archaic hominins occupied the Tibetan Plateau in the Middle Pleistocene and successfully adapted to high-altitude hypoxia environments much earlier than the regional arrival of modern *Homo sapiens*.

Main Text

Denisovans are an extinct sister group of Neanderthals, and only known from fragmentary fossils identified at a single site, Denisova Cave (Altai, Russia; Extended Data Fig. 1a). Their genomic legacy is present at relatively high frequency in several Asian, Australian and Melanesian populations[4,11–14], suggesting that they once might have been widespread. Denisovan introgression into present day Tibetans, Sherpas and neighbouring populations includes positive selection on the Denisovan allele of the Endothelial PAS domain-containing protein 1 (*EPAS1*), which provides high-altitude adaptation to hypoxia in extant humans inhabiting the Tibetan Plateau[6,15,16]. This Denisovan-derived adaptation is currently difficult to reconcile with the low altitude of Denisova Cave (700 meters above sea level, masl) and the earliest evidence of high-altitude presence of humans on the Tibetan Plateau around 30-40 thousand years before present (ka BP)[17–20]. Furthermore, the relationships of various Middle Pleistocene (MP) and Late Pleistocene (LP) hominin fossils in East Asia with Denisovans are difficult to resolve due to limited morphological information on Denisovans and the lack of paleogenetic data on MP hominin fossils from East Asia and tropical Oceania.

The right half of a hominin mandible was found in the Baishiya Karst Cave in 1980 (3200 masl; Fig. 1, Extended Data Figs. 2, 3). A recent survey revealed the presence of Palaeolithic stone artifacts in Baishiya Karst Cave (Extended Data Fig. 1b). An in-situ carbonate matrix is present on the bottom of the specimen, allowing determination of a minimum age for the Xiahe mandible. Three carbonate subsamples were collected for U-Th dating (see SI; Methods). The bulk ^{230}Th age of 164.5 ± 6.2 ka BP is not statistically different from 155 ± 15 for the uppermost and 163 ± 10 ka BP for the lowermost parts of the crust (Student *t*-test, $p < 0.05$; Extended

Data Tab. 1; SI). Consistency between the ages of the subsamples from different places of the carbonate indicates this crust formed in a short time period at 160 ka BP. Hominins therefore occupied the Tibetan Plateau at least as early as marine isotope stage (MIS) 6 in the penultimate glacial period.

There is no evidence for the preservation of ancient DNA in the Xiahe mandible (Methods). However, palaeoproteomic analysis revealed the survival of an endogenous ancient proteome in a dentine sample, but not in a bone sample (Extended Data Fig. 4; Methods;[9,21]). The endogenous proteins are highly degraded and clearly distinguishable from contaminating modern proteins (Extended Data Tab. 2; Extended Data Figs. 4, 5). Phylogenetic analysis of the recovered proteome results in a phylogenetic tree accurately reflecting great ape phylogeny, including the relationships between *H. sapiens*, Neanderthals, and Denisovans (Fig. 2). Within this framework, the Xiahe proteome is placed together with the Denisovan high-coverage genome (Denisova Cave individual D3; Bayesian probability: 0.99;[22]). In addition, the observed state of particular single amino acid polymorphisms (SAPs) within the Xiahe proteome further supports the close relationship between the Xiahe proteome and Denisovans (SI 4). Only one high-coverage Denisovan genome is currently available (D3), limiting our understanding of the proteomic sequence diversity within “Denisovans”. We therefore assign the Xiahe mandible to a hominin population closely related to the Denisovans from Denisova Cave.

The Xiahe mandible is heavily encrusted in a carbonate matrix (Extended Data Fig. 2). The carbonate matrix is the only in-situ material that can currently be directly associated with the mandible. We therefore qCT-scanned the specimen and removed the carbonate matrix

digitially (see Methods). The Xiahe mandible displays an archaic morphology that is rather common among MP hominins. Metrically, the fossil is within the variation of this group (SI Tab. 2). The body is very robust, relatively low and thick. Its height slightly decreases towards the back. The mandibular reliefs are pronounced, in particular the lateral prominence and the well-developed anterior marginal tubercle. Internally, a protruding mandibular torus overhangs a marked sub-alveolar fossa. From the mandibular foramen, the mylohyoid line runs in a rather low position. The mental foramen is located under the P_4 and rather low on the body. Although a mental trigone is weakly expressed, there is no developed chin and the symphysis is strongly receding with an inclination angle of 69° (Fig. 1d). Lingually, a primitive pattern of a small genioglossal fossa separating the upper and lower transverse tori is present. The archaic morphology of the Xiahe mandible is confirmed by geometric morphometric (GM) analysis (Extended Data Fig. 6). It falls within the hull of MP specimens and at the limit of the *Homo erectus* distribution. In contrast, it is well separated from *H. erectus* in the GM analysis of the dental arcade shape (Extended Data Fig. 7). Its arcade is less elongated than *H. erectus* and plots close to primitive forms of MP hominins, Neanderthals and *Homo sapiens*.

The dental morphology also fits the MP hominin variability. The M_1 has five well-developed primary cusps and a Y-fissure pattern. In addition, it has two accessory cusps: *tuberculum sextum* (C6) and *tuberculum intermedium* (C7; SI Tab. 4). The middle-trigonid crest is absent from the outer enamel surface (OES), but present at the enamel-dentine junction (EDJ) as a low continuous crest that dips at the sagittal sulcus (grade 2 in ref[23]; Extended Data Fig. 7). There are two wide roots – mesial and distal – each with bifurcated apices. The M_2, which was erupting but already in functional occlusion, preserves the five principal cusps arranged in a

Y-pattern, and a large C7 (SI Tab. 4). No middle-trigonid crest is present at the OES or EDJ. The principal component analysis of the EDJ ridge and cervix shape groups the Xiahe M_2 with other MP specimens such as Mauer and Balanica. It falls at the limit of the *H. erectus* distribution

The assignment of the Xiahe mandible to the Denisovans orients the morphological comparisons toward their sister group, the Neanderthals, the material from Denisova Cave, and pene-contemporaneous East Asian specimens. Xiahe lacks the high mandibular body observered in Neanderthals and its symphyseal profile is more receding than the mean values observed in this group. However, the anterior part of the arcade is flattened and similar to that observed in Neanderthals. There is also the marked retromolar space commonly observed in Neanderthals. However, this feature might be linked to the agenesis of the M_3.

The feature of the Xiahe specimen that best links it to the fragmentary fossils from the Denisova Cave is its large dentition. In shape space, the size of the Xiahe dental arcade surpasses all the comparative specimens along PC1, with the exceptions of WT15000 and Tighénif 3. The combination of a moderately large mandible with an exceptionally large dental arcade is confirmed by analysis of the teeth. The bucco-lingual diameter of the M_1 is larger than the mean of all MP samples and exceeds the maximum value of the MP European samples (SI Tab. 2; SI Fig. 2). Its mesio-distal diameter is larger than, and outside the range of, all our comparative specimens. The M_2 has a bucco-lingual diameter at the high end of the *H. erectus* range. Its mesio-distal diameter is within the range of the MP European sample but outside the range of the rest of the comparative samples (SI Tab. 3).

Among the pene-contemporaneous East Asian specimens, Xiahe is similar in several aspects to the Penghu 1 mandible[24]. The metrics of the two fossils that can be compared are very similar (SI Tab. 2) and their dental similarities are striking. Like Xiahe, Penghu 1 displays anagenesis of the M_3. Although Penghu's M_2 is smaller than that of Xiahe, in both individuals the M_2 crown is wider mesio-distally than bucco-lingualy. Xiahe's and Penghu's M_2 roots are remarkable. In addition to mesial and distal plate-like roots there is a prominent accessory lingual root that branches off the mesial root below the cervix. This feature is of particular interest as three-rooted mandibular molars are very rare in non-Asian *H. sapiens* but appear much more frequently in recent Asian populations (see SI). Finally, in both specimens, the P_3 displays Tomes' root, a feature occasionally observed in other fossil hominins (Extended Data Fig. 8a). Among other non-*sapiens* Chinese specimens, similarities with the Xujiayao[25] material should also be underlined. For example, at the EDJ, the M_2 displays a moderately complex occlusal basin, low dentine horns and a weakly expressed protostylid. These observations reinforce the idea that Denisovans are already represented in the described fossil record of China, particularly in fossils like Penghu 1 and Xujiayao. Future ancient DNA and ancient protein analysis of these specimens can directly test such hypotheses.

The Xiahe mandible is the first Denisovan found outside of Denisova Cave[1,11]. The minimum MP age of the mandible makes the Xiahe mandible comparable in age to Denisovan 2, the chronologically oldest Denisovan fossil currently known from Denisova Cave[2,3,26]. As Neanderthals and Denisovans are estimated to have diverged around 445-473 thousand years ago[27], the early part of the Denisovan lineage therefore remains undocumented in the fossil

record. However, the Xiahe mandible demonstrates that beyond the Altaï region, Denisovans or Denisovan-related populations have deep roots in central East Asia.

The Xiahe mandible represents the earliest hominin fossil on the Tibetan Plateau. It is at least 120 thousand years older than the oldest known Paleolithic sites (30-40 ka BP) in the region[17,20] (Fig. 3). Successful colonization of, and adaptation to, high-altitude plateaus like the Himalayas have generally been considered as restricted to recent *H. sapiens*[20], particularly due to resource scarcity, low temperatures, and hypoxia. In contrast, the Xiahe mandible demonstrates that archaic hominins occupied the Tibetan Plateau and successfully adapted to high-altitude environments (Fig. 3). The evidence suggests that Denisovans or Denisovan-related populations have accumulated adaptive alleles beneficial to high-altitude occupation during their presence on the Tibetan Plateau. Archaic hominin alleles in modern Himalayan populations, such as the Denisovan-derived *EPAS1* allele[6,16], may therefore derive from a local archaic hominin on or around the Tibetan Plateau, like the Xiahe hominin.

The Xiahe Denisovan provides evidence for a deep evolutionary history of these archaic hominins within the challenging environment of the Tibetan Plateau. This fossil raise the veil on the Denisovan anatomy, resolves several outstanding questions concerning this group and paves the way towards a better understanding of the MP hominin evolutionary history in East Asia.

FIGURES

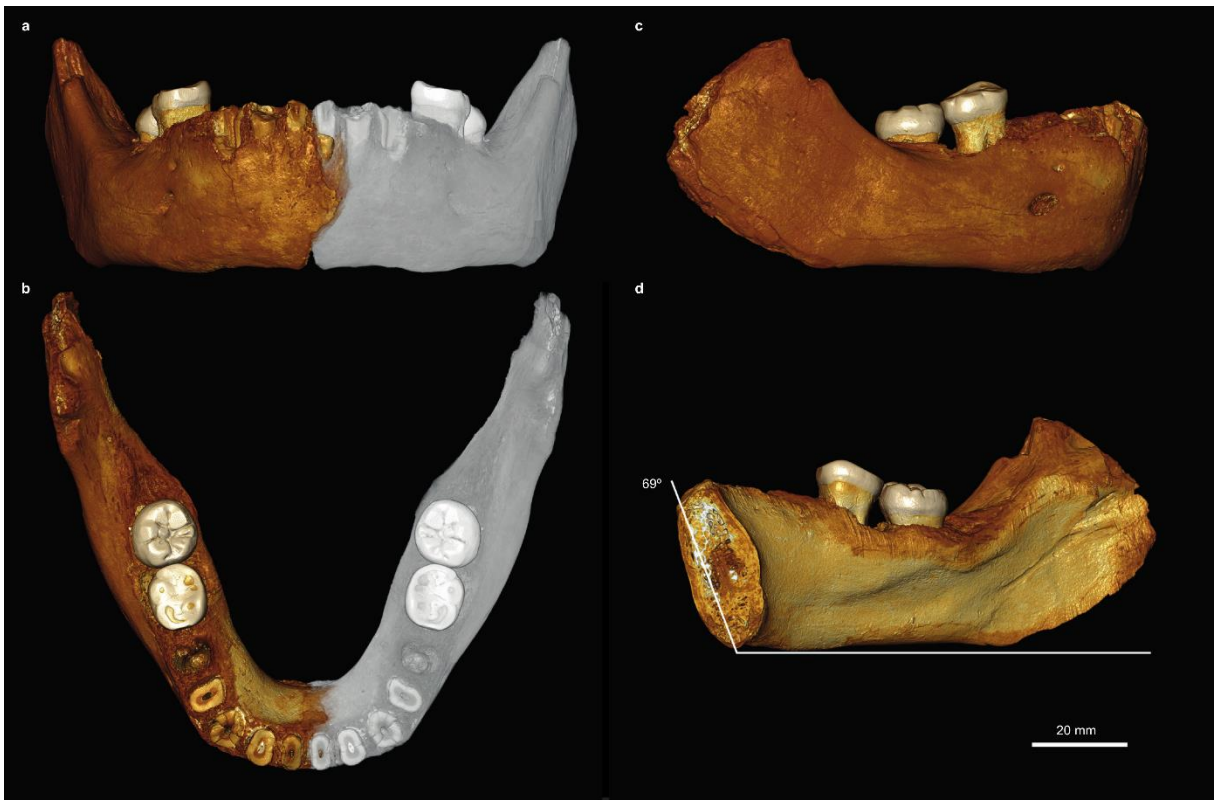

Figure 1. The Xiahe mandible. Anterior (**a**), occlusal (**b**), lateral (**c**), and internal (**d**) views of the reconstructed specimen. The preservation of the symphyseal region of the mandible allows for a virtual reconstruction of the two sides of the mandible. Mirrored parts are in gray. The symphyseal section and the infradentale-gnathion angle are displayed on **d**. See Methods for the reconstruction and Extended Data Fig. 2 for the original fossil.

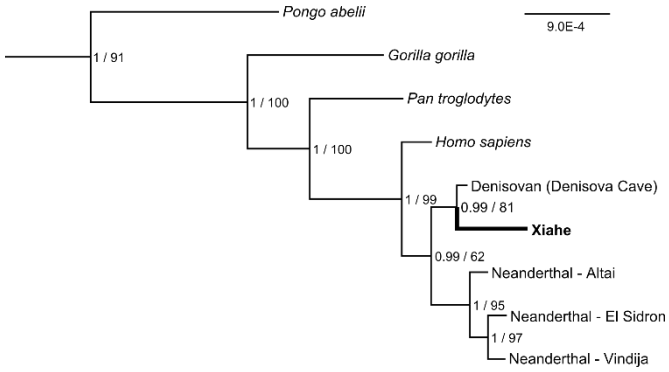

Figure 2. Phylogenetic position of the Xiahe proteome within great apes (Hominidae). Node values indicate Bayesian probability (0-1) / RAxML maximum likelihood (0-100%), respectively. *Macaca macaca* and *Nomascus leucogenys* are used as outgroups (not shown).

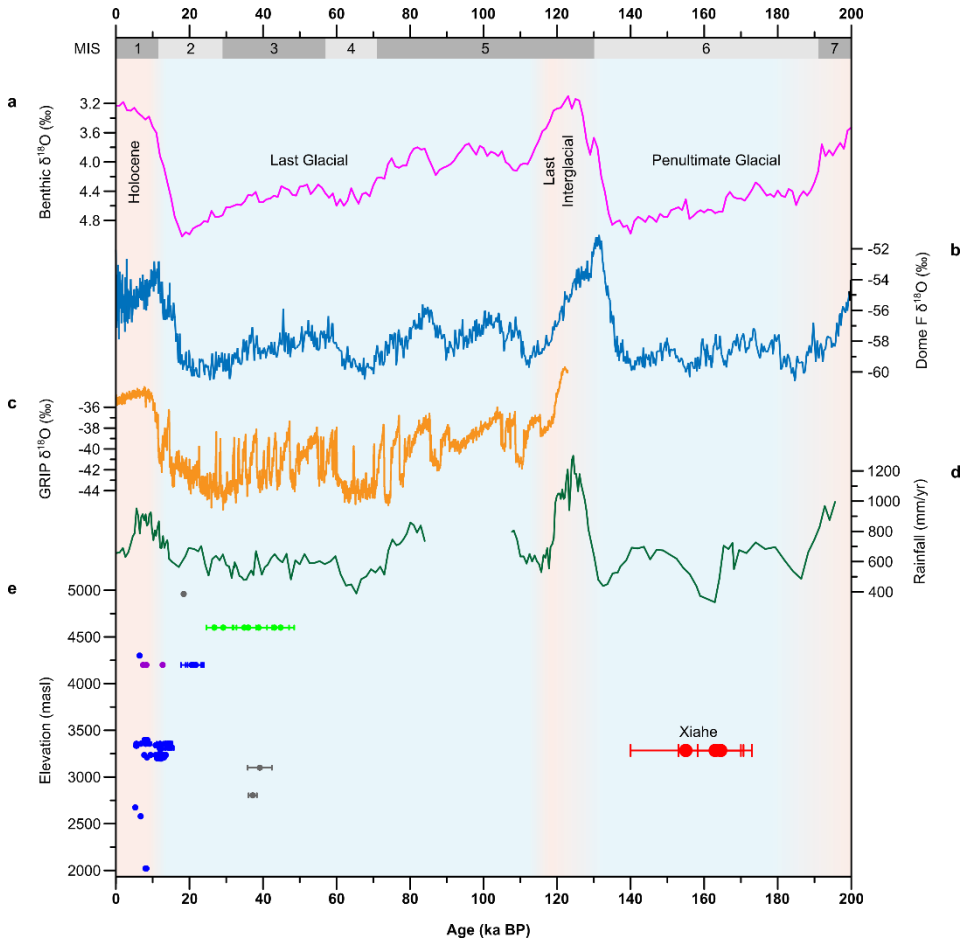

Figure 3. The paleoclimate background to human presence on the Tibetan Plateau in the past 200 thousand years. a, LR04 Benthic stack $\delta^{18}O$ records[28]. **b,** Antarctic Fuji Dome ice core $\delta^{18}O$ isotope data[29]. **c,** Greenland Ice Sheet Project (GRIP) $\delta^{18}O$ isotope data[30]. **d,** The ^{10}Be-based rainfall for Loess samples from Baoji, China[31]. **e,** Available absolute dates of Paleolithic and Epi-Paleolithic sites on the Tibetan Plateau (see Methods).

REFERENCES

1. Krause, J. *et al.* The complete mitochondrial DNA genome of an unknown hominin from southern Siberia. *Nature* **464**, 894–897 (2010).
2. Sawyer, S. *et al.* Nuclear and mitochondrial DNA sequences from two Denisovan individuals. *Proc. Natl. Acad. Sci. U. S. A.* **112**, 15696–15700 (2015).
3. Slon, V. *et al.* A fourth Denisovan individual. *Sci Adv* **3**, e1700186 (2017).
4. Browning, S. R., Browning, B. L., Zhou, Y., Tucci, S. & Akey, J. M. Analysis of Human Sequence Data Reveals Two Pulses of Archaic Denisovan Admixture. *Cell* **173**, 53–61 (2018).
5. Sankararaman, S., Mallick, S., Patterson, N. & Reich, D. The Combined Landscape of Denisovan and Neanderthal Ancestry in Present-Day Humans. *Curr. Biol.* **26**, 1241–1247 (2016).
6. Huerta-Sánchez, E. *et al.* Altitude adaptation in Tibetans caused by introgression of Denisovan-like DNA. *Nature* **512**, 194–197 (2014).
7. Chen, F. H. *et al.* Agriculture facilitated permanent human occupation of the Tibetan Plateau after 3600 B.P. *Science* **347**, 248–250 (2015).
8. Meyer, M. C. *et al.* Permanent human occupation of the central Tibetan Plateau in the early Holocene. *Science* **355**, 64–67 (2017).
9. Welker, F. Palaeoproteomics for human evolution studies. *Quat. Sci. Rev.* **190**, 137–147 (2018).
10. Welker, F. Elucidation of cross-species proteomic effects in human and hominin bone proteome identification through a bioinformatics experiment. *BMC Evol. Biol.* **18**, 23 (2018).

11. Reich, D. *et al.* Genetic history of an archaic hominin group from Denisova Cave in Siberia. *Nature* **468**, 1053–1060 (2010).
12. Qin, P. & Stoneking, M. Denisovan Ancestry in East Eurasian and Native American Populations. *Mol. Biol. Evol.* **32**, 2665–2674 (2015).
13. Skoglund, P. & Jakobsson, M. Archaic human ancestry in East Asia. *Proc. Natl. Acad. Sci. U. S. A.* **108**, 18301–18306 (2011).
14. Reich, D. *et al.* Denisova admixture and the first modern human dispersals into Southeast Asia and Oceania. *Am. J. Hum. Genet.* **89**, 516–528 (2011).
15. Jeong, C. *et al.* Admixture facilitates genetic adaptations to high altitude in Tibet. *Nat. Commun.* **5**, 3281 (2014).
16. Hackinger, S. *et al.* Wide distribution and altitude correlation of an archaic high-altitude-adaptive EPAS1 haplotype in the Himalayas. *Hum. Genet.* **135**, 393–402 (2016).
17. Zhang, D. *et al.* History and possible mechanisms of prehistoric human migration to the Tibetan Plateau. *Sci. China Earth Sci.* **59**, 1765–1778 (2016).
18. Yuan, B., Huang, W. & Zhang, D. New evidence for human occupation of the northern Tibetan Plateau, China during the Late Pleistocene. *Chin. Sci. Bull.* **52**, 2675–2679 (2007).
19. Zhao, M. *et al.* Mitochondrial genome evidence reveals successful Late Paleolithic settlement on the Tibetan Plateau. *Proc. Natl. Acad. Sci. U. S. A.* **106**, 21230–21235 (2009).
20. Zhang, X. L. *et al.* The earliest human occupation of the high-altitude Tibetan Plateau 40 thousand to 30 thousand years ago. *Science* **362**, 1049–1051 (2018).

21. Welker, F. *et al.* Palaeoproteomic evidence identifies archaic hominins associated with the Châtelperronian at the Grotte du Renne. *Proc. Natl. Acad. Sci. U. S. A.* **113**, 11162–11167 (2016).

22. Meyer, M. *et al.* A high-coverage genome sequence from an archaic Denisovan individual. *Science* **338**, 222–226 (2012).

23. Bailey, S. E., Skinner, M. M. & Hublin, J.-J. What lies beneath? An evaluation of lower molar trigonid crest patterns based on both dentine and enamel expression. *Am. J. Phys. Anthropol.* **145**, 505–518 (2011).

24. Chang, C.-H. *et al.* The first archaic Homo from Taiwan. *Nat. Commun.* **6**, 6037 (2015).

25. Xing, S., Martinón-Torres, M., Bermúdez de Castro, J. M., Wu, X. & Liu, W. Hominin teeth from the early Late Pleistocene site of Xujiayao, Northern China. *Am. J. Phys. Anthropol.* **156**, 224–240 (2015).

26. Douka, K. *et al.* Age estimates for hominin fossils and the onset of the Upper Palaeolithic at Denisova Cave. *Nature* **565**, 640–644 (2019).

27. Prüfer, K. *et al.* The complete genome sequence of a Neanderthal from the Altai Mountains. *Nature* **505**, 43–49 (2014).

28. Lisiecki, L. E. & Raymo, M. E. A Pliocene-Pleistocene stack of 57 globally distributed benthic δ18O records. *Paleoceanography* **20**, PA1003 (2005).

29. Uemura, R. *et al.* Ranges of moisture-source temperature estimated from Antarctic ice cores stable isotope records over glacial–interglacial cycles. *Clim. Past* **8**, 1109–1125 (2012).

30. Andersen, K. K. *et al.* High-resolution record of Northern Hemisphere climate extending into the last interglacial period. *Nature* **431**, 147–151 (2004).

31. Beck, J. W. *et al.* A 550,000-year record of East Asian monsoon rainfall from 10Be in loess. *Science* **360**, 877–881 (2018).

SUPPLEMENTARY INFORMATION

Supplementary Information is available in the online version of this paper.

ACKNOWLEDGEMENTS

We are grateful to the 6th Gongtang Living Buddah, Liling Wang and her husband, and Junyi Xie for providing us the opportunity to study the fossil. We thank D. Madsen, J. Brantingham, D. Rhode, C. Perreault, J. Yang, T. Cheng, X. Shen, J. Yao, Z. Yang, J. Chen and C.-R. Huang for their assistance in the fieldwork and in the laboratory. We also thank the help from the local government of Xiahe County and Ganjia town, the monks in the Baishiya temple and people from Bajiao Ancient City for their support of the fieldwork. We are grateful to O. Jöris, G. Smith, P. Ungar, R. Grün for their helpful discussions and comments. We are grateful to the many curators and colleagues who, over the years, gave us access to recent and fossil hominin specimens for computed tomography scanning, photogrammetry or analysis, to E. Trinkaus for providing comparative data, to H. Temming, S. Tuepke, C. Molenaar and Diondo GmbH, Hattigen, Germany, for their technical assistance. We thank Svante Pääbo and Aximu Ayinuer-Petri. We thank support from the Strategic Priority Research Program of Chinese Academy of Sciences, Pan-Third Pole Environment Study for a Green Silk Road (Pan-TPE) (#XDA20040000) and National Natural Science Foundation of China (#41620104007). D.J.Z. thanks the support from National Natural Science Foundation of China (#41771225). Fieldwork in 2018 was supported by the Second Tibetan Plateau Scientific Expedition (Project no. 4). U-Th dating was supported by the Science Vanguard Research Program of the Ministry of Science and Technology (#107-2119-M-002-051) and the Higher Education Sprout Project of the Ministry of Education, Taiwan (#107L901001). J.-J.H. and F.W. thank the Max Planck Society for providing financial support.

AUTHOR CONTRIBUTIONS

F.H.C., J.-J.H. and D.J.Z. designed the study. D.J.Z., G.R.D., G.H.D. H.W., J.W. and H.X. collected field data. D.J.Z., H.X. and J.W. carried out sampling and subsampling process. C.-C.S. and T.-L.Y. conducted U-Th dating of the crust carbonates. Q.M.F. performed the ancient DNA extractions. Mandibular metrical and non-metrical data were compiled and analyzed by J.-J.H. and I.B. Geometric morphometric analysis of the mandible were performed by S.E.F., S.S., I.B. and J.-J.H. Dental metrical and non-metrical data were compiled and analyzed by S.E.B. and M.M.S. F.W., R.F., S.D. and H.X. performed proteomic analysis. F.W., F.H.C., J.-J.H., D.J.Z. and C.-C.S. wrote the paper with contributions of all authors.

AUTHOR INFORMATION

The authors declare no competing financial interests.

Correspondence and requests for material should be addressed to the relevant corresponding

authors.

METHODS

Study site.

Baishiya Karst Cave, 3200 masl, is located on the south face of the Dalijiashan mountain in Ganjia Basin, Xiahe County, Gansu province, China, on the northeastern Tibetan Plateau (Extended Data Fig. 1). The cave is located at the mouth of the Jiangla River, a small tributary of Yangqu River in Ganjia Basin. This cave, with a 10 m-high and 20 m-wide entrance and several chambers, is more than 1 km long. The studied mandible fossil was found in 1980. Extensive surveys and test excavations in the cave and surrounding regions have been conducted since 2011. Animal bones and stone artifacts, including flakes, cores and scrapers were discovered in the shallow sediments of the cave entrance. Two nearby Paleolithic sites discovered in 2016 suggest that prehistoric human activity was not restricted to the cave but also present in the open-air regions of Ganjia Basin (Extended Data Fig. 1).

Chronological dates for archaeological sites on the Tibetan Plateau displayed in Figure 4 were taken from the following literature. Dates in blue (from various sites) were previously compiled by Chen et al.[7] and Madsen et al.[32]. Dates in purple (the Quesang site) are published by Meyer et al.[8]. Dates in green (the Nwya Devu site) are published in Zhang et al.[20]. Gray symbols (Wulunwula lake site, Siling Co and Lenghu sites) represent indirect and disputed dates published in Brantingham et al.[33]. Dates in red are those reported in this paper for the Xiahe mandible. This overview clearly demonstrates that the Xiahe hominin is a minimum of 120 ka older than any previously identified hominin occupation of the Tibetan Plateau.

U-Th dating.

U-Th dating was performed on one bulk sample and two serial samples of carbonate crust adhering to the Xiahe mandible (SI Fig. 1). After an ultrasonic cleaning step with ultrapure water, U-Th dating was applied to the three subsamples. Procedures were conducted in a class-10,000 clean room with class-100 benches at the High-Precision Mass Spectrometry and Environment Change Laboratory (HISPEC), Department of Geosciences, National Taiwan University[34]. Each sample was dissolved in 7 N HNO_3 and spiked with a ^{233}U-^{236}U-^{229}Th tracer, the sample solution was added to 0.2 ml $HClO_4$ and refluxed at 90-100 °C overnight for over 10 hours to decompose organic material. Uranium and thorium were purified with chemical methods including Fe co-precipitation and anion-exchange chromatography[35]. After the final column separation step the separated U and Th aliquots were further treated with 0.05-0.2 ml $HClO_4$, refluxed at 90-100 °C for over 5 hours, and dried to effectively remove organic material and reduce polyatomic interferences. U and Th fractions were then dissolved in 1% HNO_3 (+0.05% HF) for instrumental analysis[35].Determinations of all isotopic compositions and concentrations were made on a Thermo-Finnigan NEPTUNE multi-collector inductively coupled plasma mass spectrometer (MC-ICP-M)[35]. U-Th uncertainties were calculated at 2σ level. U-Th isotopic compositions, activity, and ^{230}Th dates, in years before AD 1950, with 2s error, are given in Extended Data Table 1.

Morphological Analysis.

A list of all specimens used in various morphological comparisons with extant and other fossil

hominins can be found in SI Table 6.

Computed tomography and virtual reconstruction of the fossil. The original fossil specimen was scanned using a Diondo d3 industrial micro-computed tomography scanner (Diodon GmbH) at the DCS Engineering Innovation Laboratory, Shanghai, China. The specimen was scanned with an isotropic voxel size of 52.125 µm. Segmentation of the micro-computed tomography volume was performed in Avizo (Visualization Sciences Group). The comparative dental sample was scanned with an isotropic voxel size ranging from 11.6 to 39.1 µm at the MPI EVA on a BIR ARCTIS 225/300 micro-computed tomography scanner or on a Skyscan 1172 micro-computed tomography scanner. The micro-computed tomography slices were filtered using a median filter followed by a mean-of-least-variance filter to reduce the background noise while preserving and enhancing edges. The matrix adhering to the mandible was virtually removed by manual segmentation. The specimen was reconstructed with Aviso by mirroring the right side of the mandible to the left in the position allowing the best anatomical match of the overlapping symphyseal regions.

Mandibular metric data. Three-dimensional (3D) surface models of recent *H. sapiens* and fossil mandibles were obtained from either computed tomography scans, NextEngine laser scans (Grotte des Enfants 4, Tianyuandong, Wadjak 2, Zhoukoudian Upper Cave 108 and recent *H. sapiens* Coimbra sample), or photogrammetric methods. In the latter method, two-dimensional photos (from 40 to 90) were taken per mandible with a Nikon camera. After excluding the background of each image, the photos were processed by Agisoft software. Each stack of photos ran through alignment, geometric reconstruction and texturing steps in order to become a 3D surface model. For most fossils, surface models were made from the original specimen, however in several instances research quality casts were implemented (Minatogawa A, Minatogawa 1, Sima de los Huesos XXI, Wadjak 2, Zafarraya, Zhoukoudian Upper and Lower Cave (GI/II, H1.12, Jaw K/G1.66). Linear measurements were taken on 3D surface models. Data generated through these various methods are comparable in terms of quality and precision (SI Tab. 1). Our measurements were complemented by measurements of the original specimens taken by E. Trinkaus (height and breadth of the mandibular corpus at the level of the mental foramen) and comparative data taken from the literature (see Supplementary Information).

Shape analysis of the mandible. Geometric morphometric (GM) methods were used to analyze the shape of the Xiahe mandible in a comparative context. 3D coordinates of anatomical landmarks and curve semilandmarks (n= 88) were digitized on the surface models (n= 170) using Landmark Editor[36] according to the preserved morphology of the Xiahe mandible. Landmark and semilandmark data were analyzed in R. Missing bilateral landmarks and curve semilandmarks were estimated by mirroring the preserved side. Missing landmarks and curve semilandmarks lacking a bilateral counterpart were estimated by deforming the sample average onto the deficient configuration using thin-plate spline interpolation. Curve semilandmarks were slid by minimizing the bending energy of a thin-plate spline deformation between each specimen and the sample mean shape[37,38]. After sliding, all landmarks and curve semilandmarks were converted to shape variables using a generalized Procrustes analysis.

The resulting shape coordinates were analyzed in a between-group principal component analysis (PCA). Shape changes were visualized along PC1 and PC2 by warping the sample mean shape along the positive and negative ends of PC1 and PC2, plus/minus two standard deviations (+ 2 SDVs) from the sample mean. The comparative sample composition can be found in the Supplementary Information.

Shape analysis of the dental arcade. Geometric morphometric methods were used to analyze the shape of the Xiahe mandible dental arcade. Three-dimensional landmark data were collected on computed tomographic scans and surface scans of recent *H. sapiens* (rHs) (n = 52) and fossils (n = 42). Specimens of rHs were scanned using industrial micro CT (BIR ACTIS 225/300 at the MPI-EVA, Leipzig, Germany; isotropic voxel sizes 0.03 – 0.093 mm), and medical CT (Vivantes Klinikum Berlin, Germany; CIMED, La Plata, Argentina; and the Smithsonian Institution, Washington, U.S.A.; recent human CT scans were obtained as part of Copes[39]); pixel sizes 0.13 –0.47 mm, slice intervals 0.33 - 0.50 mm). The fossil hominin samples comprise CT scans and surface scans of the original fossils and casts, which were obtained by the MPI-EVA, Leipzig, Germany. To capture mandibular arcade shape, spatial arrangement of the teeth, and dental size proportions, landmarks were taken on the alveolar margin of every tooth except the third molars. Additionally, landmarks were taken at the cervix of the first and second molars because these teeth are preserved in Xiahe. The landmarks were placed at the most distal, buccal, mesial, and lingual tooth dimensions on the alveolar bone of the incisors, canines, and premolars. For the molars, a mesial and a distal landmark, as well as two landmarks were taken at the most exposed position of the mesial and distal root. The cervical landmarks on M_1 and M_2 were placed at the most distal, buccal, mesial, and lingual position. Missing data were estimated by thin-plate spline (TPS) warping. All measurements were taken in Avizo. Landmarks were symmetrized using reflected relabeling[40] and superimposed applying the Generalized Procrustes Analysis[41,42]. To create a larger comparative sample set, we estimated mandibular arcades from maxillary arcades following the protocol described previously[43–45]. Therefore, the same landmarks protocol as described above was applied to the maxillary arcades of fossils that lack lower jaws. To estimate mandibular arcades for these individuals, we used multiple multivariate regression based on the covariation between maxillary and mandibular landmarks. To analyze differences in shape, we performed principal component analysis (PCA) on the Procrustes shape coordinates. To analyze the impact of size, we added the variable log centroid size to the Procrustes shape coordinates. The inclusion of estimated dental arcade wireframes based on available maxillary arcades (Extended Data Fig. 4) results in the same relationship of Xiahe to other hominin fossils in both shape and form space as when such estimated mandibular arcades are excluded from the analysis (SI Fig. 3). All statistical analyses were performed in Mathematica[46]. The comparative sample composition can be found in the Supplementary Information.

Dental metric and non-metric data. Crown metric and non-metric data were collected from casts or originals, with a few exceptions taken from the literature. See the Supplementary Information for details on exceptions. Root metric data were taken on 3D models generated from micro-computed tomographic data. Crown measurements were taken using Mitituyo digital callipers. Non-metric trait expressions were scored using the Arizona State University

Dental Anthropology System[47] where applicable (for lower dentition: cusp 6, cusp 7, molar groove pattern, protostylid) and Bailey et al.[23] for the middle trigonid crest. The recent *H. sapiens* sample includes individuals from southern, western and eastern Africa, western and central Europe, northeastern Asia, western Asia, India, Australia, New Guinea and Andaman Islands. For root metrics, the sample composition can be found in the Supplementary Information.

Molar EDJ shape analysis. Enamel and dentine tissues (Extended Data Fig. 5) of lower second molars were segmented using the 3D voxel value histogram and its distribution of greyscale values[48,49]. After segmentation, the EDJ was reconstructed as a triangle-based surface model using Avizo. Small EDJ defects were corrected digitally using the "fill holes" module of Geomagic Studio. We then used Avizo to digitize 3D landmarks and curve-semilandmarks on these EDJ surfaces[48,49]. Anatomical landmarks were placed on the tip of the dentine horn of the protoconid, metaconid, entoconid and hypoconid. A sequence of landmarks was also placed along the marginal ridge connecting the dentine horns beginning at the top of the protoconid moving in lingual direction; the points along this ridge curve were then later resampled to the same point count on every specimen using Mathematica. Likewise, we digitized and resampled a curve along the cemento–enamel junction as a closed curve starting and ending below the protoconid horn and the mesiobuccal corner of the cervix. The resampled points along the two ridge curves were subsequently treated as sliding curve semilandmarks and analyzed using GM together with the four anatomical landmarks. The comparative sample composition can be found in the Supplementary Information.

Ancient DNA analysis.

We prepared one extract from 64.3 mg of dentine powder from the Xiahe mandible, as described in Dabney et al.[50]. From this extract (10 µl out of 50 µl), we produced one library using a single-stranded library protocol[22,51]. We captured human mitochondrial DNA genome sequences (mtDNA) from this library using the in-solution capture method described in Fu et al.[52] to determine the DNA preservation. We sequenced the enriched library on a MiSeq using a double index configuration (2x76bp) and merged the forward and reverse sequences into a single fragment requiring an overlap of at least 11 bp. We mapped these merged reads, which we call a "fragment", to the revised Cambridge reference sequence (rCRS NC_012920) using bwa[53] with the following parameters: –n 0.01 and –l 16500. We removed duplicate fragments by identifying all fragments with the same start and end positions and keeping the one with the highest average base quality.

We observe no ancient damage pattern, which suggests that the Xiahe mandible does not contain ancient human DNA. Deamination of cytosine (C) to uracil (U) residues occurs primarily at single-stranded DNA overhangs and leaves characteristic patterns of C→T substitutions in sequences obtained from ancient DNA molecules because uracils are read as thymines (T) by DNA polymerases. When we measured the number of fragments that contain C->T substitutions relative to the mtDNA consensus sequence, we find that this value is 0.4-0.7%. When we only take fragments with C->T substitutions in the first or last position, the frequency of C->T substitutions at the other end of the fragment is 2.1-3.7%. In conclusion, this mandible shows no evidence suggesting the presence of ancient human DNA.

Ancient protein analysis.

Protein Extraction. Separate bone and dentine samples (SI Fig. 1) were drilled at the Key Laboratory of Western China's Environmental Systems (Ministry of Education) in Lanzhou University, China. Dentine and bone samples were treated using established proteome extraction protocols[21,54]. This resulted in an ammonium-bicarbonate fraction (hereafter AmBic) and acid-demineralization fraction (hereafter Acid) for each sample. An extraction blank followed the exact same extraction procedure to estimate protein contamination during protein extraction and analysis in Lanzhou, Leipzig, and Oxford.

MALDI-TOF-MS. MALDI-TOF-MS analysis followed protocols established elsewhere[21,54,55]. Positive MALDI spectra were obtained for the dentine fractions in the low molecular range (<2500 m/z) only. AmBic and Acid extractions of the bone sample returned negative MALDI spectra in all cases. Only the Acid and AmBic fractions of the dentine sample were therefore analyzed using shotgun proteomics at the University of Oxford, UK.

LC-MS/MS. Samples were analyzed on an Orbitrap Fusion Lumos in tandem with an Ultimate 3000 RSLCnano UPLC (both Thermo Fisher Scientific). Chromatographic separation of peptides was achieved on an EASY Spray PepMAP UHPLC column (50 cm x 75 μm, 2 μm particle size) after trapping on a PepMAP u-pre-column (0.5 cm x 300 μm). Peptides were eluted with a linear gradient of 5 -35% acetonitrile in 5% DMSO/0.1% formic acid, followed by column washing and equilibration steps. Each sample was followed by a blank injection to evaluate sample carry-over. MS1 spectra were acquired between 400 and 1500 Th in the orbitrap detector with a resolution of 120,000 and an AGC target of 400,000. Selected precursors were excluded for 7 seconds before repeated analysis in the Orbitrap at a resolution of 15,000 and after HCD fragmentation (28% normalized collision energy). Precursors were isolated in the quadrupole with an isolation window of 1.2 Th. The instrument used a top speed duty cycle (3 seconds) with a maximum injection time of 40 ms and AGC target of 40,000.
LC-MS/MS analysis of the AmBic and Acid fractions was conducted on three separate occasions. AmBic and Acid extracts were analyzed separately as well, resulting in six ancient protein files. In addition to injection blanks, extraction blanks were analyzed twice, again preceding and followed by injection blanks. All these remained empty of appreciable amounts of proteins, only including common laboratory contaminants.

Data analysis. Mass spectrometry files (.raw) from ancient samples, extraction blanks and injection blanks were converted to .mgf files using ProteoWizard[56]. Files resulting from the same extraction were searched together in PEAKS v. 7.[57]. Deamidation (NQ), oxidation (M), hydroxylation (P), pyro-glu (EQ,) and phosphorylation (HCDRSTY) were selected as variable modifications. MS1 tolerance was set at 10 ppm and MS2 tolerance at 0.07 Da. Peptides were only accepted with an FDR equal to 1.0% or lower, with a minimum of 2 unique peptides for each protein with a total score of -10lgP ≥ 20. The first search was run against the entire human proteome database with the addition of Neanderthal- and Denisovan-specific protein sequences for a selected set of common bone and dentine proteins. The acceptance of amino acid substitutions in comparison to the provided sequence database followed the guidelines

presented by Welker[10]. Example MS/MS spectra of phylogenetically informative sequences can be found in SI Figure 4. The database was supplemented with a list of proteins commonly suspected to represent contaminants proteins[58].

For MALDI-TOF-MS spectra, glutamine deamidation was quantified for P1105, the collagen peptide appearing at an m/z of 1105.6, as this is a slow-deamidation peptide frequently observed in collagen MALDI-TOF-MS spectra[59]. For LC-MS/MS datasets, the extent of glutamine and asparagine deamidation was calculated as the ratio of spectra containing deamidated glutamine and/or asparagine positions to the total number of spectra containing glutamine and/or asparagine positions for each protein identified individually[21]. Contamination-filtering left eight collagens as likely endogenous the Xiahe dentine proteome (Extended Data Tab. 2).

In addition to deamidation, we utilized a similar approach based on peptide-spectrum-matches (PSM) spectral counts to get an insight into peptide cleavage sites (both N- and C-termini of each peptide). One would expect modern proteins to have few, or no, non-enzymatic cleavages, while proteins preserved for extended periods of time might have undergone hydrolysis. Such hydrolysis would appear as non-proteotypic cleavage in resulting fragmention spectra. We normalized the obtained PSM counts in comparison to a random cleavage model for each investigated protein. To this end, human reference sequences for 12 selected proteins were randomly cleaved, N- and C-terminal amino acid cleavage windows (positions P1 and P1') obtained for all the PSMs matching a particular protein, and the observed percentage divided by the theoretical percentage for random cleavage for each protein. We observe a large amount of semi-tryptic or non-tryptic peptide-spectrum-matches in the endogenous collagens while such peptide-spectrum-matches are almost absent in contaminants (Extended Data Fig. 7). In addition, for the endogenous collagens we observe a far greater enrichment of cleavages after arginines (R, mainly R.G cleavages) compared to lysines (K, mainly K.G cleavages). The source of this difference is unclear, although a similar difference does not seem to be present for the contamination proteins. Therefore, its source may lie in diagenetic modifications of lysines, for example lysine methylation, making this residue inaccessible to trypsin cleavage.

Phylogenetic Analysis. Of those proteins endogenous to the Xiahe dentine sample, six proteins were used for subsequent phylogenetic analysis (*COL1α1*, *COL1α2*, *COL2α1*, *COL3α1*, *COL5α1* and *COL5α2)*. Proteins *COL9α1* and *COL11α2* were excluded as these had a low number of matching peptides in both the Acid and AmBic extractions (Extended Data Tab. 2). *COL10α1* sequences were added to these as we previously demonstrated the highly informative protein sequences of this gene within archaic hominins[21]. Protein sequence alignments were aligned with the homologous sequences from all great ape genera and translated protein sequences from ancient hominin genomes (Neanderthals[60] and a Denisovan[61]), while a macaque (*Macaca mulatta*) and a gibbon (*Nomascus leucogenys*) were used as outgroups. See SI Table 5 for accession numbers.

Phylogenetic trees were built on the CIPRES Science Gateway[62] using MrBayes Bayesian phylogenetic analysis and RAxML maximum-likelihood methods. The protein sequence alignment was partitioned by gene for both analyses, allowing for variable substitution rates between genes using the Dayhoff substitution model. MrBayes was run for 5 million

generations, with sampling every 500 generations, and 10% burn-in discarded, while RAxML was run for 1,000 bootstrap iterations.

Code availability.

All R code used to generate protein deamidation and peptide cleavage patterns are available upon request to Dr. Frido Welker.

Data deposition.

All the proteomic mass spectrometry data have been deposited in the ProteomeXchange Consortium repository with the identifier PXDXXXXXX. Protein consensus sequences for the Xiahe hominin used for phylogenetic analysis are available in Supplementary File 2. A surface scan model of the Xiahe mandible is publicly available at: XXXX.

METHODS REFERENCES

32. Madsen, D. B. *et al.* Early foraging settlement of the Tibetan Plateau highlands. *Archaeological Research in Asia* **11**, 15–26 (2017).
33. Brantingham, J. P. *et al.* A short chronology for the peopling of the Tibetan Plateau. in *Developments in Quaternary Sciences* **9**, 129–150 (Elsevier, 2007).
34. Shen, C.-C. *et al.* Variation of initial 230Th/232Th and limits of high precision U–Th dating of shallow-water corals. *Geochim. Cosmochim. Acta* **72**, 4201–4223 (2008).
35. Shen, C.-C. *et al.* High-precision and high-resolution carbonate 230Th dating by MC-ICP-MS with SEM protocols. *Geochim. Cosmochim. Acta* **99**, 71–86 (2012).
36. Wiley, D. F. *et al.* Evolutionary morphing. (2005).
37. Gunz, P., Mitteroecker, P. & Bookstein, F. L. Semilandmarks in Three Dimensions. in *Modern Morphometrics in Physical Anthropology* (ed. Slice, D. E.) 73–98 (Springer US, 2005).
38. Gunz, P. & Mitteroecker, P. Semilandmarks: a method for quantifying curves and surfaces. *Hystrix, the Italian Journal of Mammalogy* **24**, 103–109 (2013).
39. Copes, L. Comparative and Experimental Investigations of Cranial Robusticity in Mid-Pleistocene Hominins. (Arizona State University, 2012).
40. Mardia, K. V., Bookstein, F. L. & Moreton, I. J. Statistical assessment of bilateral symmetry of shapes. *Biometrika* **92**, 249–250 (2005).
41. Rohlf, F. J. & Slice, D. Extensions of the Procrustes Method for the Optimal Superimposition of Landmarks. *Syst. Biol.* **39**, 40–59 (1990).
42. Bookstein, F. L. *Morphometric Tools for Landmark Data: Geometry and Biology*. (Cambridge University Press, 1997).
43. Stelzer, S., Gunz, P., Neubauer, S. & Spoor, F. Using the covariation of extant hominoid upper and lower jaws to predict dental arcades of extinct hominins. *J. Hum. Evol.* **114**, 154–175 (2018).
44. Stelzer, S., Neubauer, S., Hublin, J.-J., Spoor, F. & Gunz, P. Morphological trends in arcade shape and size in Middle Pleistocene Homo. *Am. J. Phys. Anthropol.* (2018). doi:10.1002/ajpa.23721
45. Spoor, F. *et al.* Reconstructed Homo habilis type OH 7 suggests deep-rooted species diversity in early Homo. *Nature* **519**, 83–86 (2015).

46. Mathematica, V. *5.1 (Wolfram Research Inc., Champaign, IL, 2004)*.
47. Turner, C. G. Scoring procedures for key morphological traits of the permanent dentition: the Arizona State University dental anthropology system. *Advances in dental anthropology. New York: Wiley-Liss. p* 13–31 (1991).
48. Skinner, M. M., Gunz, P., Wood, B. A. & Hublin, J.-J. Enamel-dentine junction (EDJ) morphology distinguishes the lower molars of Australopithecus africanus and Paranthropus robustus. *J. Hum. Evol.* **55**, 979–988 (2008).
49. Skinner, M. M., Gunz, P., Wood, B. A., Boesch, C. & Hublin, J.-J. Discrimination of extant Pan species and subspecies using the enamel--dentine junction morphology of lower molars. *American Journal of Physical Anthropology* **140**, 234–243 (2009).
50. Dabney, J. *et al.* Complete mitochondrial genome sequence of a Middle Pleistocene cave bear reconstructed from ultrashort DNA fragments. *Proc. Natl. Acad. Sci. U. S. A.* **110**, 15758–15763 (2013).
51. Gansauge, M.-T. & Meyer, M. Single-stranded DNA library preparation for the sequencing of ancient or damaged DNA. *Nat. Protoc.* **8**, 737–748 (2013).
52. Fu, Q. *et al.* DNA analysis of an early modern human from Tianyuan Cave, China. *Proc. Natl. Acad. Sci. U. S. A.* **110**, 2223–2227 (2013).
53. Li, H. & Durbin, R. Fast and accurate short read alignment with Burrows–Wheeler transform. *Bioinformatics* **25**, 1754–1760 (2009).
54. Welker, F., Soressi, M., Rendu, W., Hublin, J.-J. & Collins, M. J. Using ZooMS to identify fragmentary bone from the late Middle/Early Upper Palaeolithic sequence of Les Cottés, France. *J. Archaeol. Sci.* **54**, 279–286 (2015).
55. Welker, F. *et al.* Variations in glutamine deamidation for a Châtelperronian bone assemblage as measured by peptide mass fingerprinting of collagen. *STAR: Science & Technology of Archaeological Research* **3**, 15–27 (2017).
56. Chambers, M. C. *et al.* A cross-platform toolkit for mass spectrometry and proteomics. *Nat. Biotechnol.* **30**, 918–920 (2012).
57. Zhang, J. *et al.* PEAKS DB: de novo sequencing assisted database search for sensitive and accurate peptide identification. *Mol. Cell. Proteomics* **11**, M111.010587 (2012).
58. Hendy, J. *et al.* A guide to ancient protein studies. *Nat Ecol Evol* **2**, 791–799 (2018).
59. van Doorn, N. L., Wilson, J., Hollund, H., Soressi, M. & Collins, M. J. Site-specific deamidation of glutamine: a new marker of bone collagen deterioration. *Rapid Commun. Mass Spectrom.* **26**, 2319–2327 (2012).
60. Castellano, S. *et al.* Patterns of coding variation in the complete exomes of three Neandertals. *Proc. Natl. Acad. Sci. U. S. A.* **111**, 6666–6671 (2014).
61. Meyer, M. *et al.* Nuclear DNA sequences from the Middle Pleistocene Sima de los Huesos hominins. *Nature* **531**, 504–507 (2016).
62. Miller, M. A., Pfeiffer, W. & Schwartz, T. Creating the CIPRES Science Gateway for inference of large phylogenetic trees. in *Gateway Computing Environments Workshop (GCE)* 1–8 (ieeexplore.ieee.org, 2010).
63. Hiess, J., Condon, D. J., McLean, N. & Noble, S. R. 238U/235U Systematics in terrestrial uranium-bearing minerals. *Science* **335**, 1610–1614 (2012).

64. Cheng, H. *et al.* Improvements in 230Th dating, 230Th and 234U half-life values, and U–Th isotopic measurements by multi-collector inductively coupled plasma mass spectrometry. *Earth Planet. Sci. Lett.* **371-372**, 82–91 (2013).
65. Jaffey, A. H., Flynn, K. F., Glendenin, L. E., Bentley, W. C. t. & Essling, A. M. Precision measurement of half-lives and specific activities of 235U and 238U. *Phys. Rev. C Nucl. Phys.* **4**, 1889–1906 (1971).
66. Welker, F. *et al.* Middle Pleistocene protein sequences from the rhinoceros genus Stephanorhinus and the phylogeny of extant and extinct Middle/Late Pleistocene Rhinocerotidae. *PeerJ* **5**, e3033 (2017).

EXTENDED DATA TABLES

Extended Data Table 1. U-Th ages of the crust attached on Xiahe mandible. Analytical errors are 2σ of the mean.

Subsample ID	Weight g	^{238}U 10^{-6} g/g [a]	^{232}Th 10^{-6} g/g	$\delta^{234}U$ measured [a]	$[^{230}Th/^{238}U]$ activity [c]	$^{230}Th/^{232}Th$ atomic (x 10^{-6})	Age (ka) uncorrected	Age (ka BP) corrected [c,d]	$\delta^{234}U_{initial}$ corrected [b]
XH-SD-U1	0.2198	1348.5 ± 2.1	316.0 ± 4.2	431.1 ± 2.7	1.195 ± 0.020	84.1 ± 1.8	168.3 ± 6.1	164.5 ± 6.2	686 ± 13
XH-SD-U4	0.1837	1523.2 ± 2.8	330 ± 12	388.5 ± 2.6	1.122 ± 0.052	85.4 ± 5.0	158 ± 15	155 ± 15	601 ± 28
XH-SD-U6	0.1962	1464.1 ± 2.5	477 ± 16	411.2 ± 2.7	1.177 ± 0.031	59.5 ± 2.5	169 ± 10	163 ± 10	652 ± 19

[a] $[^{238}U] = [^{235}U] \times 137.818$ (±0.65‰) (ref.[63]); $\delta^{234}U = ([^{234}U/^{238}U]_{activity} - 1) \times 1000$.

[b] $\delta^{234}U_{initial}$ corrected was calculated based on ^{230}Th age (T), i.e., $\delta^{234}U_{initial} = \delta^{234}U_{measured} X e^{\lambda 234 * T}$, and T is corrected age.

[c] $[^{230}Th/^{238}U]_{activity} = 1 - e^{-\lambda 230 T} + (\delta^{234}U_{measured}/1000)[\lambda_{230}/(\lambda_{230} - \lambda_{234})](1 - e^{-(\lambda 230 - \lambda 234) T})$, where T is the age. Decay constants are 9.1705×10^{-6} yr^{-1} for ^{230}Th, 2.8221×10^{-6} yr^{-1} for ^{234}U (ref.[64]), and 1.55125×10^{-10} yr^{-1} for ^{238}U (ref.[65]).

[d] Age corrections, relative to 1950 AD, were calculated using an estimated initial atomic $^{230}Th/^{232}Th$ ratio of $4 (\pm 2) \times 10^{-6}$.

Extended Data Table 2. Endogenous protein coverage statistics.

	AmBic		Acid		Combined		
Protein	Peptides	Unique	Peptides	Unique	Coverage (%)	N_Deam (%)	Q_Deam (%)
COL1α1	539	499	375	349	61.1 (88.2)	99.2 (733)	91.8 (2018)
COL1α2	346	338	243	236	54.8 (73.8)	98.0 (1368)	92.7 (280)
COL2α1	78	38	61	38	25.2	89.7 (29)	95.6 (247)
COL3α1	34	28	7	4	7.0	0 (8)	83.3 (18)
COL5α1	7	5	6	4	2.6	-	100 (3)
COL5α2	28	22	27	24	11.1	72.73 (11)	96.9 (96)
COL9α1	3	3	-	-	-	-	100 (9)
COL11α2	7	4	5	4	-	-	87.5 (8)

Triple-helical coverage is indicated in parentheses for *COL1α1* and *COL1α2* as the non-triple-helical regions of *COL1α1* and *COL1α2* are not present in the mature COL1 protein, and therefore not observed in most proteome studies. N_Deam: asparagine deamidation. Q_Deam: glutamine deamidation. Number of spectra (PSMs) covering asparagine and glutamine are indicated in parentheses for both deamidation columns.

EXTENDED DATA FIGURES

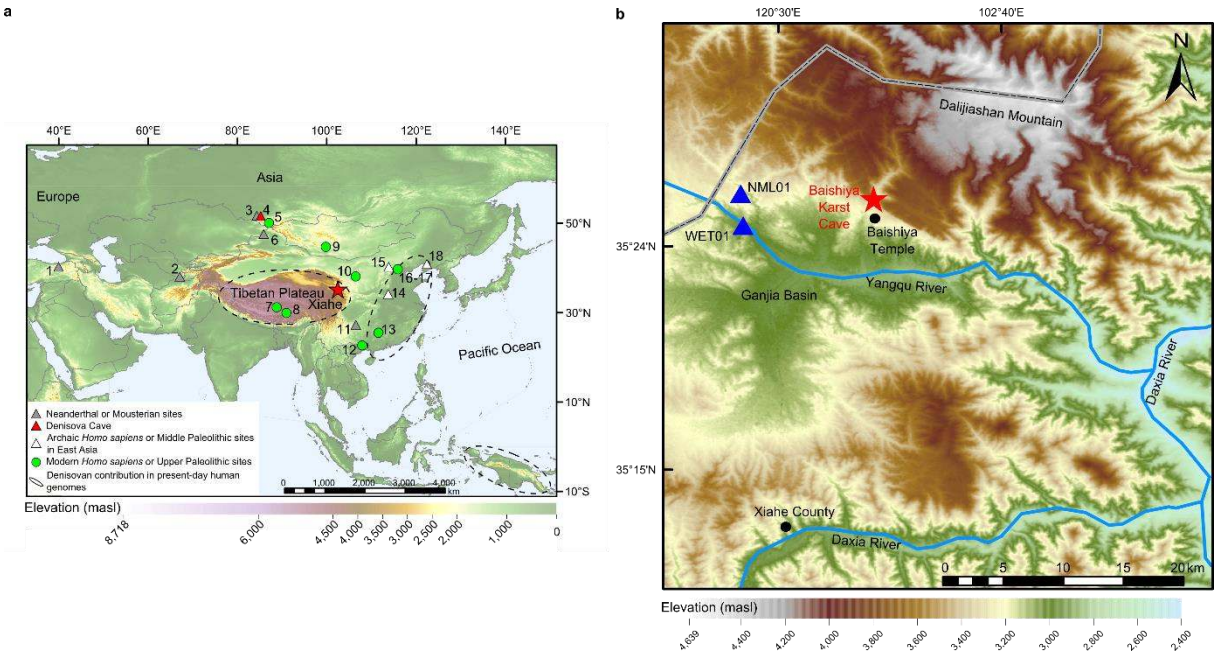

Extended Data Figure 1. Location of Baishiya Karst Cave. **a**, Location of Baishiya Karst Cave, archaic *Homo* sites, and selected Middle and Upper Paleolithic sites in East and Central Asia. Numbers denoting the archaeological sites are: 1. Mezmaiskaya Cave, 2. Teshik-Tash Cave, 3. Okladnikov Cave, 4. Denisova Cave, 5. Kara-Bom, 6. Tongtian Cave, 7. Nyadem, 8. Quesang, 9. Chikhen Agui, 10. Shuidonggou, 11. Guanyin Cave, 12. Zhiren Cave, 13. Fuyan Cave, 14. Lingjing, 15. Xujiayao, 16. Tianyuan Cave, 17. Zhoukoudian Upper Cave, 18. Jinniushan. **b**, Ganjia Basin with the Bashiya Karst Cave (red star) and two paleolithic sites (NML01, Nimalong01; WET01, Waerta01; blue triangles).

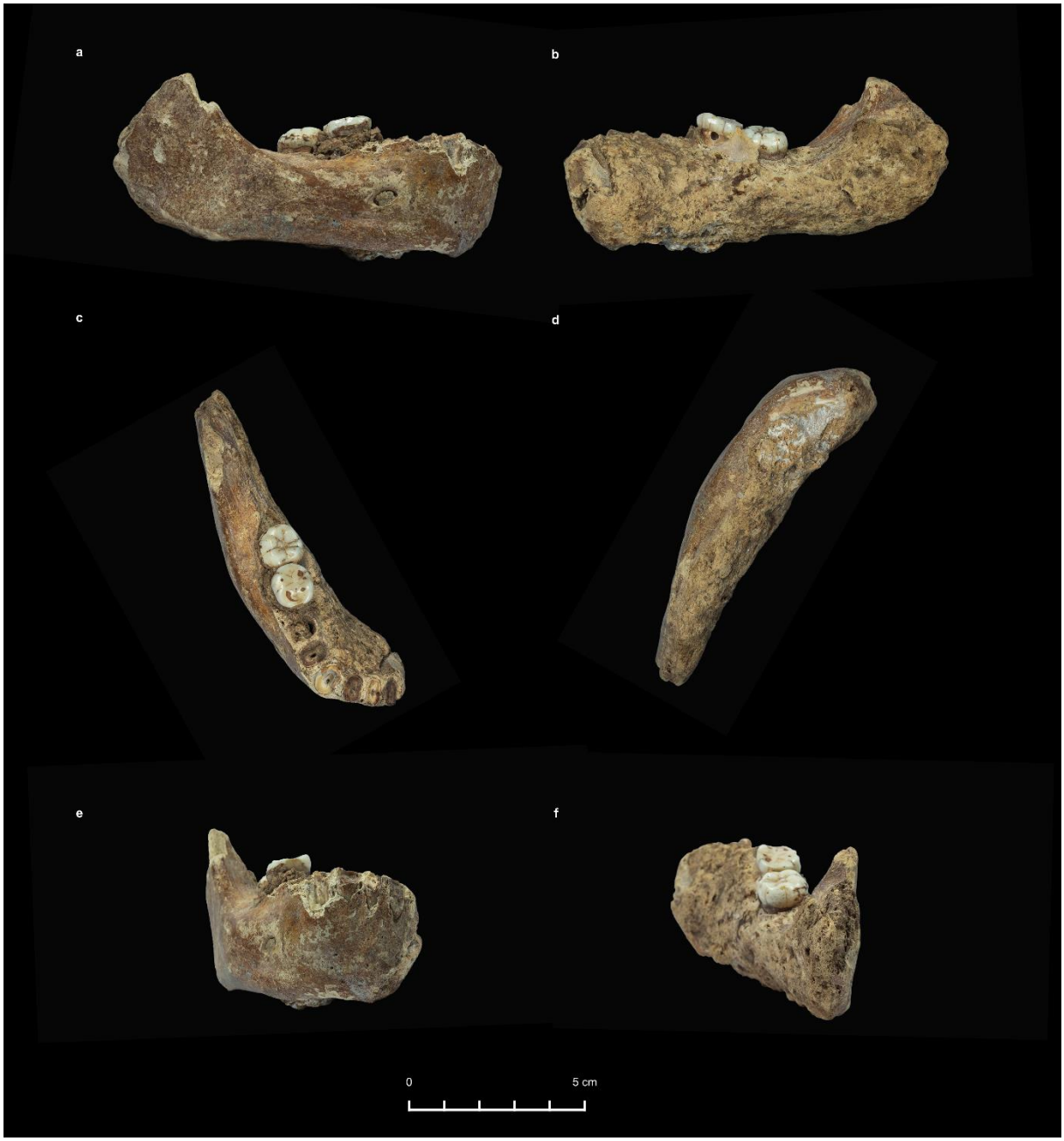

Extended Data Figure 2. Xiahe mandibular preservation with adhering calcareous crust. **a**, lateral, **b**, buccal, **c**, occlusal, and **d**, inferior, **e**, anterior **f**, posterior views. Sampling locations for ancient proteins and ancient DNA can be seen on the M_2 and ascending ramus, and sampling location for U-Th dating on the inferior surface.

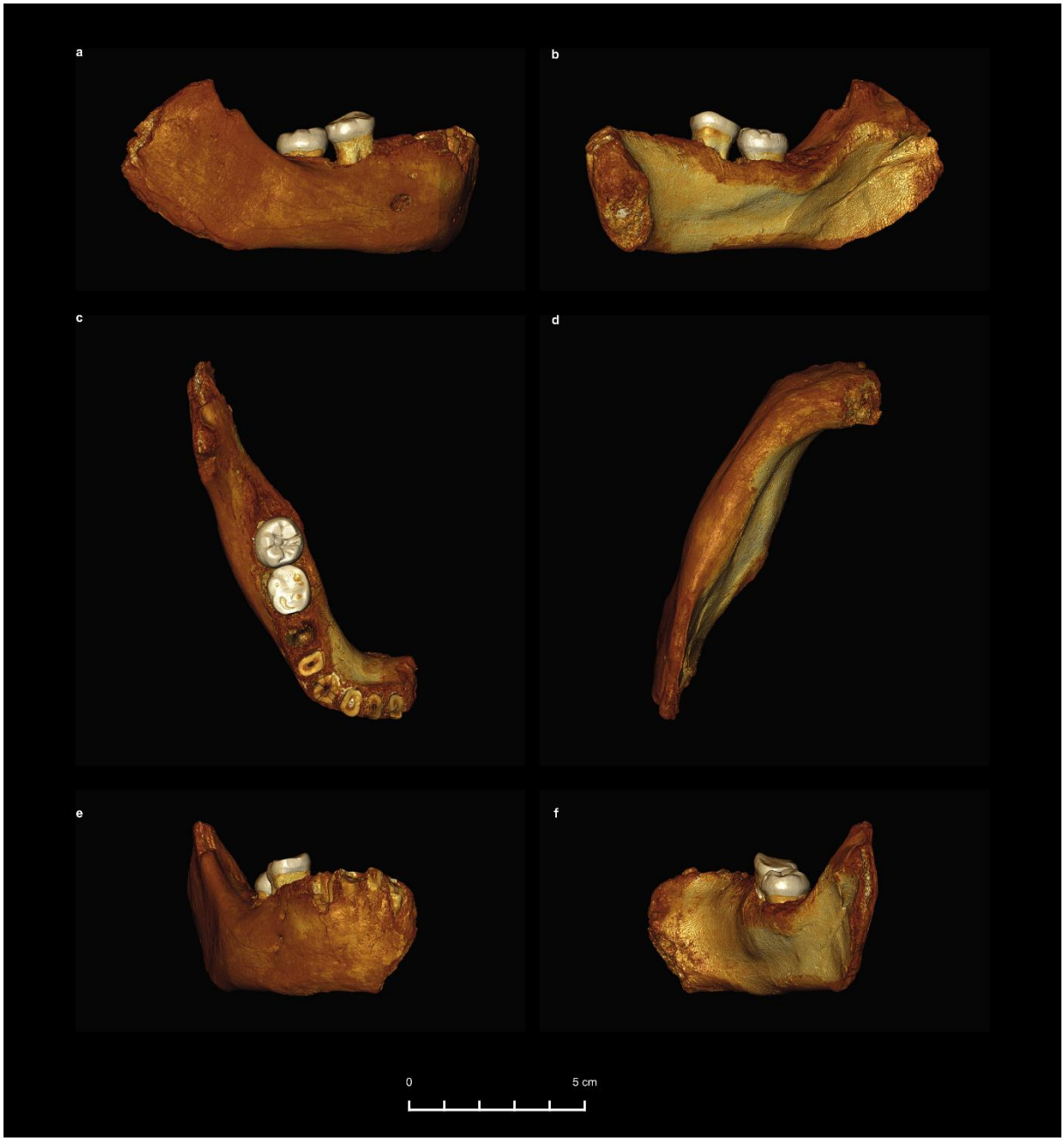

Extended Data Figure 3. Surface model of the Xiahe mandible after digital removal of the adhering calcareous crust. a, lateral, **b**, buccal, **c**, occlusal, and **d**, inferior, **e**, anterior **f**, posterior views.

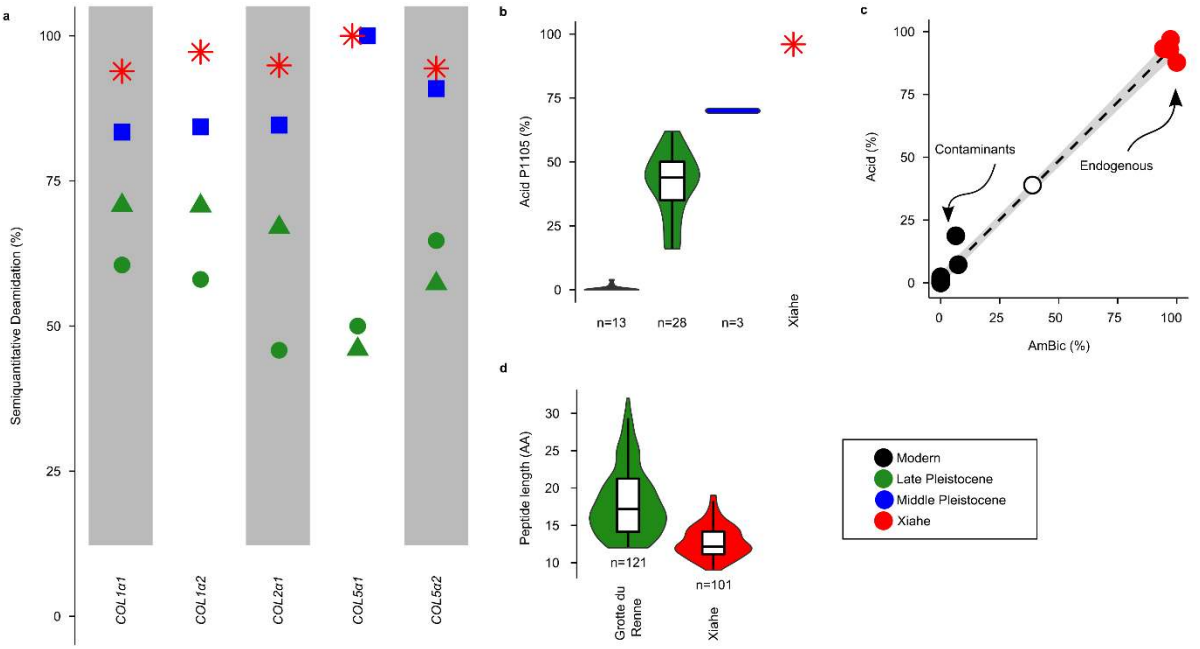

Extended Data Figure 4. Preservation of the Xiahe dentine proteome. a, Deamidation of five Xiahe proteins also identified in several LP and MP proteomes. **b,** Glutamine deamidation of peptide P1105 observed in the ZooMS analysis of the Xiahe dentine sample compared to reference data. **c,** Correlation between deamidation observed in LC-MS/MS experiments for AmBic and Acid extracts (R^2=0.99). **d,** Length distribution of non-tryptic peptides in a LP Neanderthal and the Xiahe dentine proteome. Samples are colour-coded according to geological age. Deamidation is based on quantitative MALDI-TOF-MS analysis (**b**) or on semi-quantitative spectral counting methods (**a, c**). 0% indicates an absence of deamidation and 100% indicates complete deamidation of asparagine and glutamine. Reference data:[21,54,55,66].

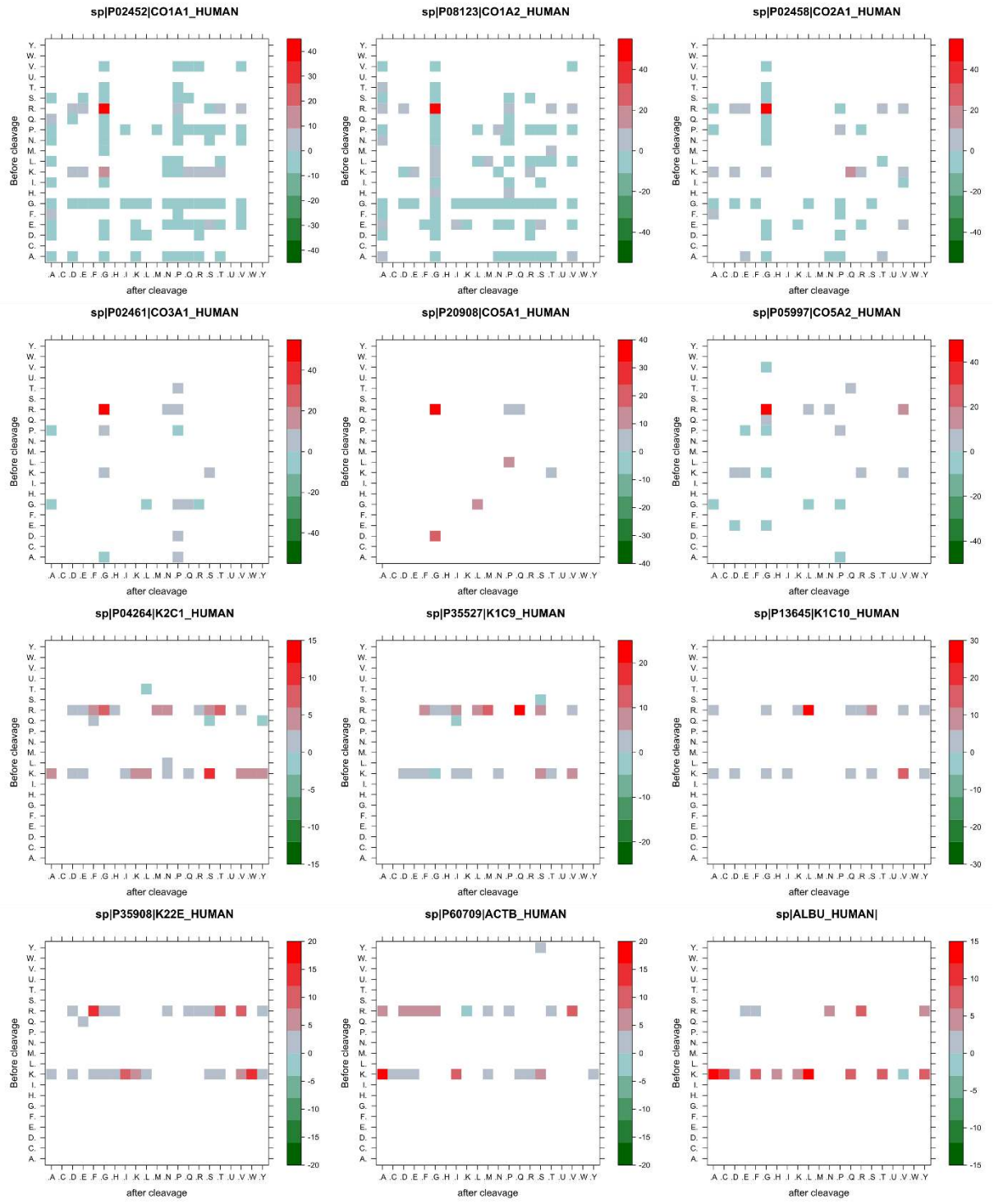

Extended Data Figure 5. Normalized frequencies of peptide cleavage patterns of selected proteins. Spectral counts are based on the total number of AmBic and Acid peptide-spectrum matches (PSMs) and include both N- and C- termini of each aligned PSM. Red colours indicate more PSMs than expected and green colours fewer PSMs than expected, compared to a random cleavage model for each protein. Note differences in colour scale.

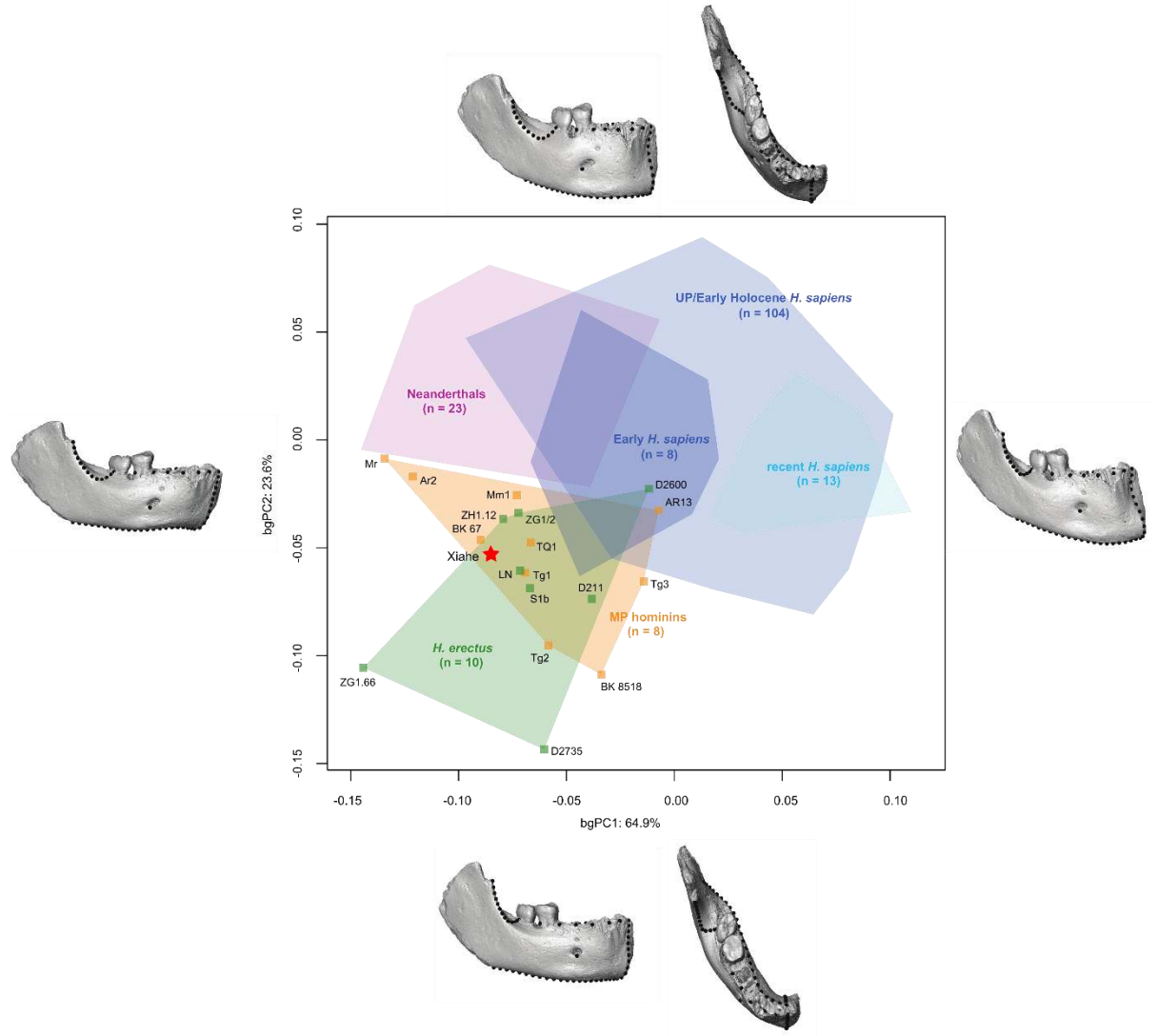

Extended Data Figure 6. Geometric morphometrics of the mandible. A between-group principal component analysis of mandibular shape. Although some overlap exists, all groups show a distinct mandibular shape. Xiahe plots at the edge of the *H. erectus* distribution and within the range of Middle Pleistocene *Homo*. Surface models illustrate mandibular shape changes along PC1 (lateral view) and PC2 (lateral and superior view). Recent *H. sapiens* are shown in cyan, Upper Palaeolithic and Holocene *H. sapiens* in light blue, early *H. sapiens* in dark blue, Neanderthals in pink, *H. erectus* in green, and other Middle Pleistocene fossil hominins in orange.

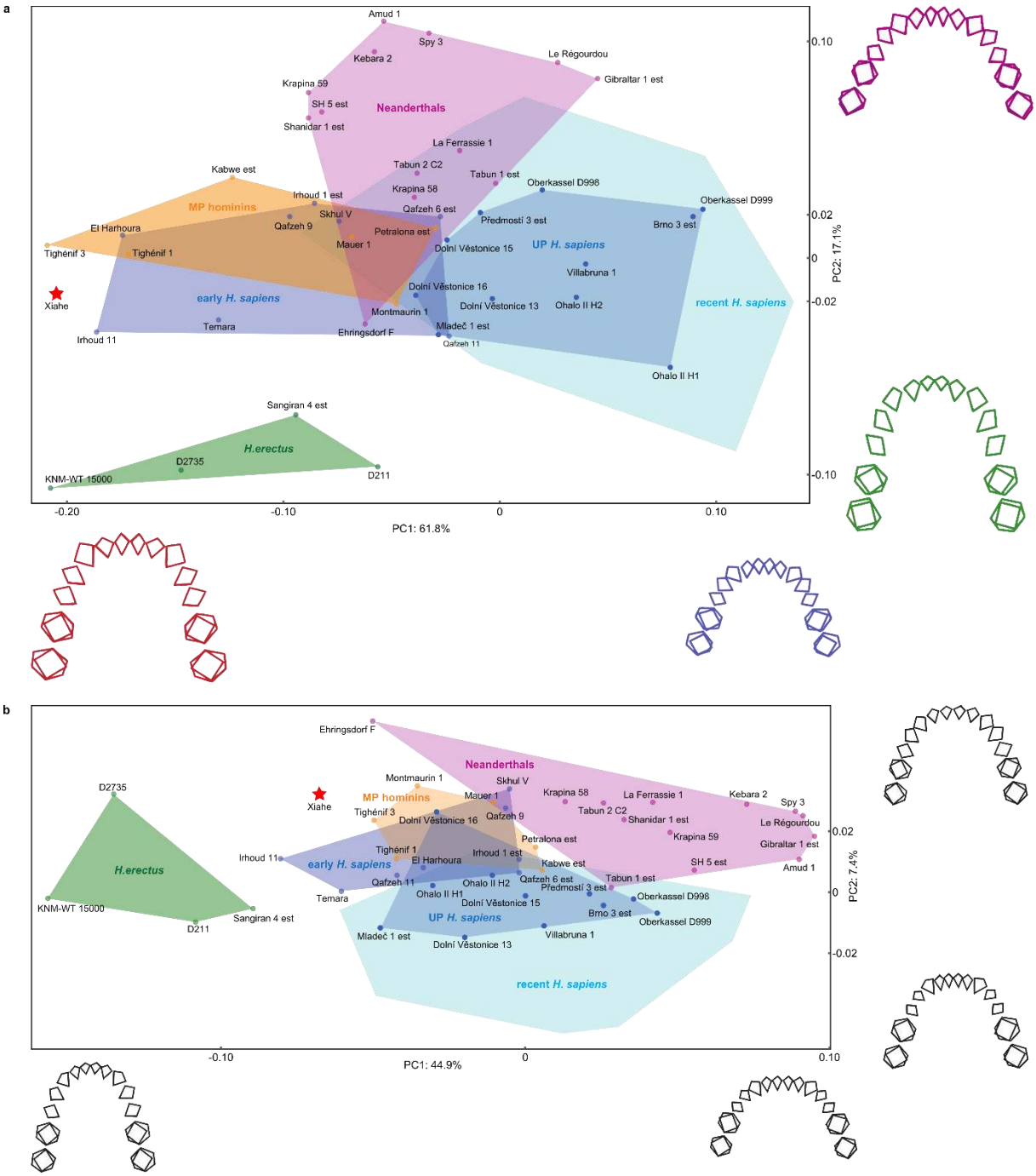

Extended Data Figure 7. Geometric morphometrics of the dental arcade. a, Procrustes form space. **b,** Procrustes shape space. The wireframes illustrate form changes along PC1 and PC2. For **a** and **b**, colours are as in Extended Data Fig. 4. The wireframes show the form and shape changes along PC1 and PC2, respectively. Estimated wireframes used in the PCA are indicated by “est”.

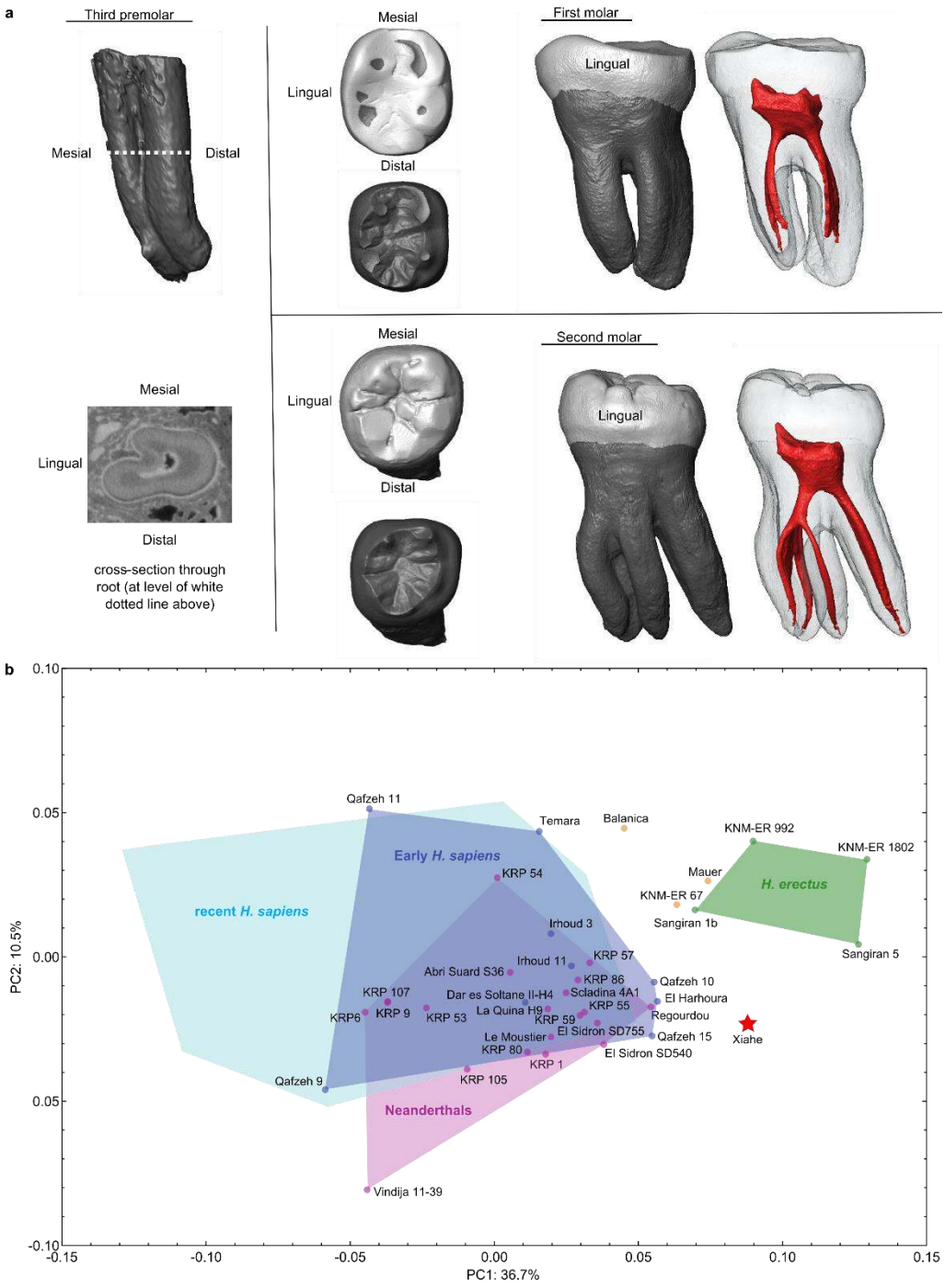

Extended Data Figure 8. Root morphology and enamel-dentine junction (EDJ) shape. a, The roots of the M_1 are typical of lower molars with a mesial and distal plate-like root. There are mesial and distal plate-like roots on the M_2; however, there is an additional accessory lingual root that splits off distally from the mesial root about 2/3 from the cervix. The P_3 root is a Tomes' form with a distinct lingual groove. **b**, A principal component analysis of EDJ ridge and cervix shape reveals a clear separation between *H. erectus* on one side and Neanderthals and *H. sapiens* on the other side, with Middle Pleistocene hominins in between. Xiahe also falls between the *H. erectus* hull and Neanderthals+*H. sapiens*, but not with the other included Middle Pleistocene specimens. Colours are as in Extended Data Fig. 4 for relevant groups.